



Kinematic partitioning in the Southern Andes (39° S–46° S) inferred from lineament analysis and reassessment of exhumation rates

Paul Leon Göllner¹ · Jan Oliver Eisermann¹ · Catalina Balbis² · Ivan A. Petrinovic² · Ulrich Riller¹

Received: 18 April 2020 / Accepted: 3 June 2021 / Published online: 8 July 2021
© The Author(s) 2021

Abstract

The Southern Andes are often viewed as a classic example for kinematic partitioning of oblique plate convergence into components of continental margin-parallel strike-slip and transverse shortening. In this regard, the Liquiñe-Ofqui Fault Zone, one of Earth's most prominent intra-arc deformation zones, is believed to be the most important crustal discontinuity in the Southern Andes taking up margin-parallel dextral strike-slip. Recent structural studies, however, are at odds with this simple concept of kinematic partitioning, due to the presence of margin-oblique and a number of other margin-parallel intra-arc deformation zones. However, knowledge on the extent of such zones in the Southern Andes is still limited. Here, we document traces of prominent structural discontinuities (lineaments) from the Southern Andes between 39° S and 46° S. In combination with compiled low-temperature thermochronology data and interpolation of respective exhumation rates, we revisit the issue of kinematic partitioning in the Southern Andes. Exhumation rates are maximal in the central parts of the orogen and discontinuity traces, trending predominantly N–S, WNW–ESE and NE–SW, are distributed across the entire width of the orogen. Notably, discontinuities coincide spatially with large gradients in Neogene exhumation rates and separate crustal domains characterized by uniform exhumation. Collectively, these relationships point to significant components of vertical displacement on these discontinuities, in addition to horizontal displacements known from published structural studies. Our results agree with previously documented Neogene shortening in the Southern Andes and indicate orogen-scale transpression with maximal vertical extrusion of rocks in the center of the transpression zone. The lineament and thermochronology data call into question the traditional view of kinematic partitioning in the Southern Andes, in which deformation is focused on the Liquiñe-Ofqui Fault Zone.

Keywords Kinematic partitioning · Liquiñe-Ofqui Fault Zone · Southern Andes · Transpression

Introduction

Kinematic partitioning of deformation at obliquely convergent plate margins into margin-orthogonal shortening and margin-parallel strike-slip components in the upper plate is a well-accepted tectonic model for many subduction and collisional orogens (e.g., Fitch 1972; Beck 1983; Kimura 1986; McCaffrey 1992). In these models, margin-parallel slip is thought to be resolved either on distributed strike-slip faults or on a limited number of prominent wrench faults,

often localized within magmatic arcs and leading to the horizontal detachment and margin-parallel displacement of one or more elongate crustal slivers in the forearc (Jarrard 1986; Beck 1991; Tikoff and Teyssier 1994; Chemenda et al. 2000; Hoffmann-Rothe 2006).

In the Central and Southern Andes, prominent margin-parallel fault zones have been attributed to kinematic partitioning (Dewey and Lamb 1992; Scheuber and González 1999; Reutter et al. 1996; Cembrano et al. 2000, 2002; Hoffmann-Rothe et al. 2006) caused by oblique subduction of the Farallon and Nazca plates below the South American plate at angles between 10° and 30° (Pardo-Casas and Molnar 1987; Somoza 1998; Chen et al. 2019). Among those fault zones, the 1200 km long Liquiñe-Ofqui Fault Zone (LOFZ) in the Southern Andes is commonly viewed as the prime example of a highly localized intra-arc fault zone accommodating margin-parallel slip between 39° S and 47° S (Fig. 1; Hervé 1976;

✉ Paul Leon Göllner
paul.leon.gollner@uni-hamburg.de

¹ Institut für Geologie, Universität Hamburg, Bundesstraße 55, 20146 Hamburg, Germany

² CICTERRA (CONICET-UNC), Av. Vélez Sarsfield 1611, Córdoba, Argentina

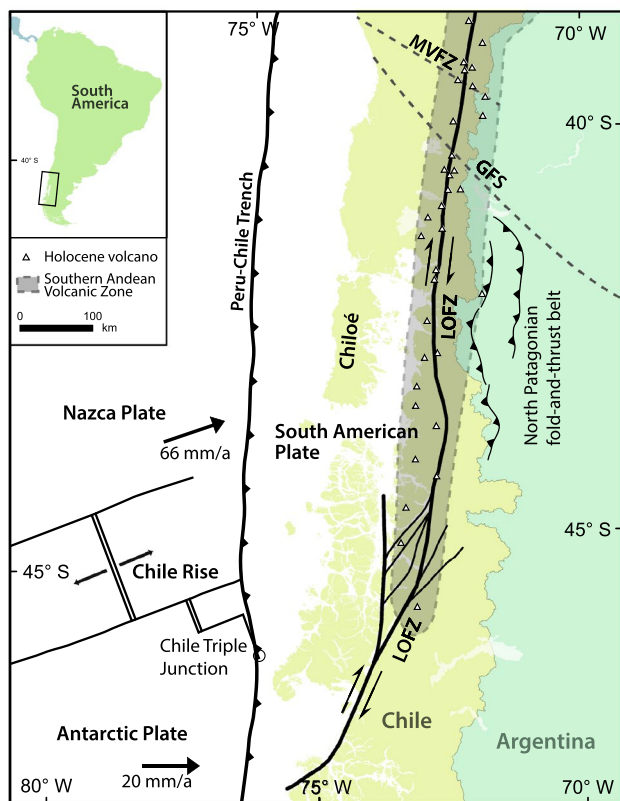


Fig. 1 Tectonic setting of the Southern Andes between 40° S and 48° S. Black arrows indicate plate motions of the Nazca and Antarctic plates relative to South America. LOFZ Liquiñe- Ofqui Fault Zone, MVFZ Mocha Villarica Fault Zone, GFS Gaste Fault System

Cembrano et al. 1996). Located within the Southern Andean Volcanic Zone (SVZ), the LOFZ separates the Chiloé area, commonly regarded as a forearc sliver, from the rest of the Andean orogen to the east of this fault zone (Fig. 1; Hervé 1976; Cembrano et al. 1996, 2000; Lavenu and Cembrano 1999). Due to the apparent northward displacement of crust underlying this area with regard to rocks east of the LOFZ (Wang et al. 2007), a major component of dextral strike-slip is attributed to the LOFZ (Cembrano et al. 1996, 2000; Wang et al. 2007). This slip component agrees with the obliquity in plate convergence (Pardo-Casas and Molnar 1987; Angermann et al. 1999; Wang et al. 2007), the GPS velocity field (Klotz et al. 2001; Moreno et al. 2011), earthquake focal mechanisms (Lange et al. 2008; Sielfeld et al. 2019a) and principal directions of paleostress inferred from fault-slip analysis (Cembrano et al. 1996; Lavenu and Cembrano 1999; Potent 2003; Rosenau et al. 2006). In the context of this tectonic framework, the LOFZ is commonly regarded as a sub-vertically dipping, narrow fault zone consisting of two NNE-trending lineaments that are connected through a number of step-over faults south of 43° S (Fig. 1; Lavenu and Cembrano 1999; Cembrano et al. 2000, 2002; Catalán et al. 2017).

Traditionally, kinematic models of intra-arc deformation in the Southern Andes strongly focus on the strike-slip kinematics of the LOFZ as the main, or even the only, fault zone accommodating margin-parallel slip in this region (Cembrano et al. 1996, 2000; Lavenu and Cembrano 1999). Recent paleomagnetic and kinematic studies, however, are at variance with the hypothesis of a single fault taking up most of the margin-parallel slip component (Rosenau et al. 2006; Hernandez-Moreno et al. 2014; Stanton-Yonge et al. 2016). Testing models of kinematic partitioning in the Southern Andes, notably within the SVZ, is hampered by a lack of comprehensive structural data, especially from the southern portion of the LOFZ, as this area is most difficult to access. Here, we address intra-arc deformation in the southern portion of the SVZ by integrating new data on traces of prominent structural discontinuities (lineaments) inferred from remote sensing with exhumation rates compiled from published low-temperature thermochronology studies. We find that kinematic partitioning in the Southern Andes is more complex than accounted for by the traditional partitioning hypothesis and is in agreement with orogen-scale transpression. This tectonic scenario sheds new light on the role of the LOFZ in the SVZ.

Previous structural studies of the SVZ

The Liquiñe-Ofqui fault zone and forearc

Initially, the LOFZ was viewed as two co-linear, continental margin-parallel morphologic lineaments representing prominent faults, connected through NE-striking step-over faults south of 43° S (Fig. 1; Hervé 1976). Cembrano and Hervé (1993) interpreted the en-échelon geometry of the step-over faults as a crustal-scale duplex. Micro-fabric analysis of rocks from three transects across the main LOFZ-lineaments revealed (1) mylonites indicating sinistral oblique-reverse step-over faults at 39° S, (2) brittle faults formed by shortening and dextral strike-slip faults at 41° S–42° S, and (3) a dextral mylonite zone at 42° S–43° S (Cembrano et al. 2000). Similarly, Cembrano et al. (2002) provided micro-structural evidence from the western master lineament and duplex shear zones for dextral displacement, but pointed out that displacement on these ductile deformation zones is also characterized by dip-slip, collectively amounting to dextral transpression south of 43° S. Furthermore, geochronological and fault-slip studies provide evidence for Neogene dextral displacement on the LOFZ (Hervé et al. 1993; Cembrano et al. 2000, 2002; Lagabrielle et al. 2004). Thermochronological studies, in particular, point to the presence of thrust faults that are kinematically associated with Miocene transpression at the southernmost LOFZ (Thomson 2002; Georgieva et al. 2016). Finally, Arancibia et al. (1999) and Lara et al. (2008) attributed significant shortening and

dextral strike-slip to transpression, based on geomorphologic and kinematic studies.

Paleomagnetic studies apparently indicate mainly counter-clockwise vertical-axis rotations of up to 170° west of the LOFZ and predominantly clockwise rotation up to 150°–170° east of the LOFZ during the Cenozoic (Beck 1991; Cembrano et al. 1992; Rojas et al. 1994; Beck et al. 1998, 2000; Garcia et al. 2011; Hernandez-Moreno et al. 2014). Regional fault-kinematic studies by Potent (2003), Potent and Reuther (2001), Rosenau (2004) and Rosenau et al. (2006) revealed a number of first-order faults with variable kinematics, collectively pointing to complex intra-arc deformation in the northern SVZ. Following the tectonic concept of Riller and Oncken (2003) for the Central Andes, Rosenau et al. (2006) proposed a kinematic model explaining up to 120 km of margin-parallel displacement through segmentation of upper crust into rhomb-shaped domains defined by margin-parallel dextral and WNW-striking sinistral faults. Recent identification of morphological lineaments and paleomagnetic studies by Hernandez-Moreno et al. (2014) corroborate the large heterogeneity of deformation in the SVZ. These authors attribute differential counter-clockwise vertical-axis rotations of fault-bound domains to distributed deformation in the Chiloé area.

The Southern Andean retroarc

The retroarc zone of the Southern Andes comprises the eastern slopes of the main cordillera. Between 41° S and 44° S, deformation in this zone formed the North Patagonian fold-and-thrust belt (Fig. 1), characterized by N- and NW-striking faults (e.g., Diraison et al. 1998; Giacosa and Heredia 2004; Orts et al. 2012; Echaurren et al. 2016). At 41° S, fault-slip analyses indicate reverse displacement on NW-striking faults and right-lateral displacement on N-striking faults (Diraison et al. 1998). Similarly, the retroarc south of 44° S is segmented by Cretaceous to Cenozoic NW-striking sinistral strike-slip and reverse faults, and N-striking dextral strike-slip faults (Diraison et al. 2000; Lagabrielle et al. 2004). Based on microtectonic analyses, Lagabrielle et al. (2004) infer a Miocene phase of horizontal shortening accomplished on NW-striking thrust faults. In summary, the formation of the North Patagonian fold-and-thrust belt is attributed to two contractional phases, one spanning from the late Cretaceous to early Paleocene and the other in the Miocene (Orts et al. 2012, 2015; Echaurren et al. 2016).

Methods

Lineament extraction

Morphological traces of planar structural discontinuities, i.e., lineaments, in the Southern Andes between 39° S and

46° S were extracted from high-resolution ASTER GDEM 2 digital elevation models (DEMs) with 30 m horizontal resolution, provided as 1 degree squares. To process this data, we developed a workflow tailored for data preparation and lineament extraction (Fig. 2). Individual DEMs were first merged to a single continuous DEM covering the entire study area. To precisely identify lineaments from the elevation models, three derivative datasets, each of which highlighting different attributes of the DEM, were calculated from the merged elevation model using the Spatial Analyst toolbox in ArcGIS (Esri). A hillshade model was calculated to enhance the contrast of elevation changes utilizing the tool *Hillshade*. Next, an aspect map, illuminating the directions facing individual slopes, was calculated using the tool *Aspect* and served to identify lineaments defined by uniform slope orientations. As erosion enhances the morphology of lithological and structural elements, a drainage map was included in the workflow. The drainage network was derived from the DEM using a combination of the tools *Fill* and *Flow accumulation*. Lineaments were then extracted from shaded relief models, drainage and aspect maps. Lineament extraction from high-resolution base maps as used in this study may easily result in oversampling of an enormous number of small-scale lineaments, which are difficult to interpret in terms of orogen-scale deformation. Lineament extraction was thus restricted to lineaments defined by major changes in the morphology within the main cordillera, such as steep valleys and prominent ridge lines with a length exceeding few tens of kilometers. In many cases, multiple datasets returned identical lineaments, which enhanced the confidence in the extraction procedure. As rivers and glaciers in the Southern Andes drain predominantly to the West and to the East, E-trending escarpments are morphologically exaggerated. Therefore, we chose to exclude these escarpments from our lineament analysis.

Exhumation rates in the SVZ

To better understand the variation in extrusion of rocks and the possible presence of vertical displacements of structural discontinuities inferred from remote sensing in the Southern Andes, we compiled published fission track (AFT) and (U–Th)/He apatite ages from Thomson et al. (2010), Georgieva et al. (2016) and Christeleit et al. (2017). Ages were converted to rock exhumation rates, which we regard as proxy to rock extrusion, applying the eroding half-space model by Willet and Brandon (2013). This model accounts for the cooling rate-dependence of closure temperatures, the advection of heat during exhumation of rocks and the transient increase of the geothermal gradient with erosion. To convert thermochronology data to exhumation rates, knowledge of the surface temperature, geothermal gradient, mean elevation of the area of interest, and the elevation, at which the sample was

obtained, was required. Furthermore, the age of onset of erosion needed to be specified. In our case, the onset of erosion was set to 130 Ma, to include all measured AFT and (U–Th)/He ages and a mean surface temperature of 7 °C (Fick and Hijmans 2017) was used for our calculation of exhumation rates. Following Thomson (2002), the geothermal gradient was estimated at 23–45 °C/km, based on an average surface heat flow of 80–112 mW/m² and the thermal conductivity of granite. The latter surface heat flow approximates well felsic intrusive rocks of the Patagonian Batholith. A mean geothermal gradient of 34 °C/km was, therefore, applied to the model. The deviation of modelled exhumation rates within the range of estimated geothermal gradients is given in Supplementary Fig. 1. To obtain representative mean elevation values, the study area was divided into six sectors (Fig. 3). Mean elevations were calculated for each from DEMs. In the cases, in

which multiple apatite grains were used to obtain (U–Th)/He ages, the unweighted mean age was used for conversion to exhumation rates. Calculated exhumation rates were subsequently interpolated by means of inverse-distance weighting (Watson and Philip 1985) using the respective errors in the underlying age as weighting factor. To highlight the variation in exhumation rates across prominent lineaments, swath profiles in E–W- and N–S-directions with a width of 10 km, each consisting of 50 individual, evenly spaced profile lines, were generated (Fig. 7).

Model limitations

We note that the calculation of exhumation rates from a large dataset, as presented in this study, requires some assumptions regarding the exhumation and the geothermal gradient that

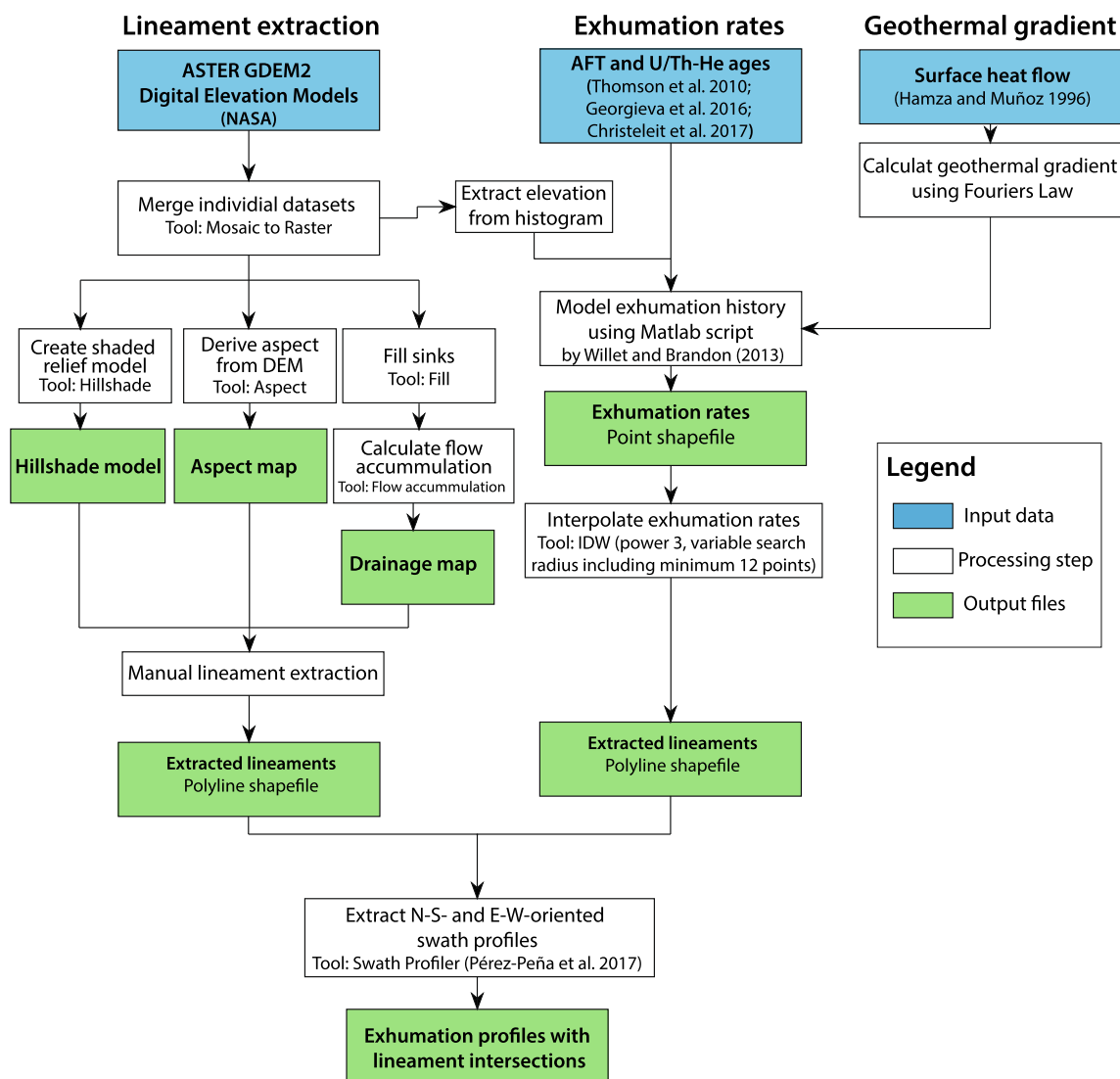
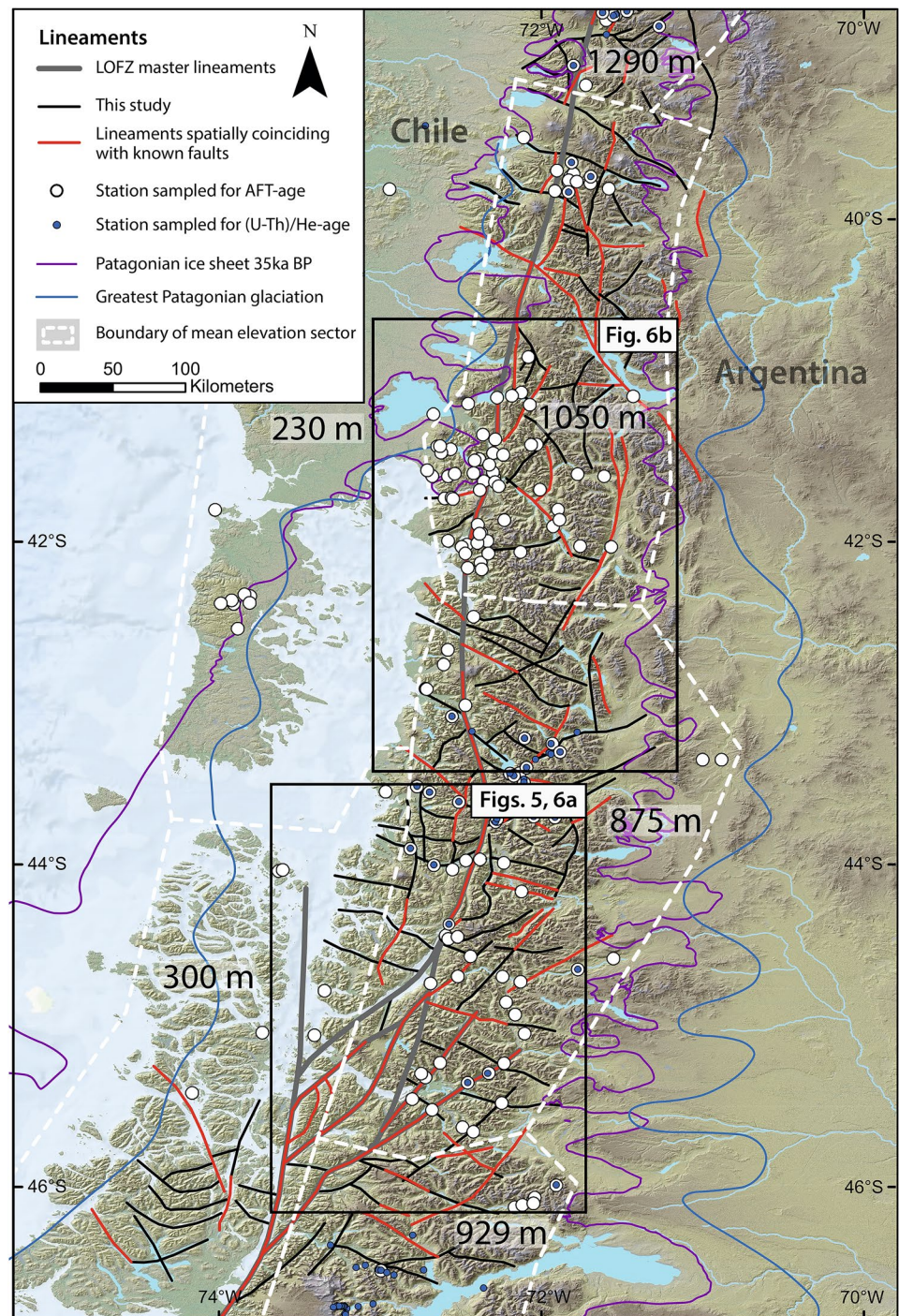


Fig. 2 Diagram illustrating the applied workflow for lineament extraction and interpolation of exhumation rates from apatite fission track and (U–Th)/He ages. For explanation see text

Fig. 3 Map of the Southern Andean Volcanic Zone investigated showing lineaments identified in this study and stations of low-T thermochronology data compiled from Thomson et al. (2010), Geogieva et al. (2016) and Christeleit et al. (2017). Lineaments coinciding with mapped faults are compiled from Diraison et al. (1998); Sernageomin (2003); Lagabrielle et al. (2004); Orts et al. (2012) and Echaurren et al. (2016). Master lineaments of the LOFZ are from Thomson (2002). White dashed lines indicate sector boundaries used for mean elevation calculation. Respective mean elevation values are given for each sector. Greatest Patagonian glaciation and Patagonian ice sheet at 35 ka are from Hein et al. (2011) and Davies et al. (2020), respectively



may affect the magnitude of calculated exhumation rates. The eroding half space model applied in this study implies a constant erosion rate from the time of closure of the respective thermochronometric system. Based on age-elevation profiles, Thomson et al. (2010) and Christeleit et al. (2017) inferred a period of enhanced exhumation at 1–7 Ma and 5–10 Ma, respectively, for the Southern Andes which is attributed to Miocene and Pliocene enhanced glaciation. We note that our orogen-scale exhumation model does not account for

the observation of local increased rock exhumation during the late Miocene and Pliocene. Age-elevation relationships of all available data do not show any meaningful trend of measured AFT and (U–Th)/He ages with elevation for the entire study area, thus, preventing a comprehensive correction for enhanced exhumation during the Miocene and Pliocene resulting from enhanced glaciation (Supplementary Fig. 2). Notably, Paleozoic and Mesozoic ages obtained at low elevations do not permit the calculation of exhumation

rates corrected for accelerated exhumation in the Pliocene under a realistic geothermal gradient, as proposed by Willet and Brandon (2013). Consequently, exhumation rates calculated from samples characterized by AFT and (U–Th)/He ages older than 10 Ma may yield lower exhumation rates than comparable exhumation rates calculated with correction for locally increased exhumation due to enhanced glaciation (Thomson et al. 2010). As we assume uniform erosion rates since the closure of the AFT and the (U–Th)/He systems, calculated exhumation rates do not account for changes in exhumation related to changes in the style of deformation, proposed for the Southern Andes (see the previous section).

As demonstrated by Willet and Brandon (2013), the conversion of AFT and (U–Th)/He ages to exhumation rates is sensitive to the selected mean elevation and geothermal gradient. Sensitivity tests based on the selection of different geothermal gradients (Supplementary Fig. 1) underscores a strong dependence of the output exhumation rate on the geothermal gradients. A spatial change of the geothermal gradient may, thus, have a strong influence on calculated exhumation rates. Sensitivity tests also show that all samples within the range of measured ages undergo the same change in exhumation rate with changing geothermal gradient (Supplementary Fig. 1). Tests exploring the influence of errors in AFT and (U–Th)/He ages on the resulting exhumation rates show a linear correlation between increasing error and resulting changes in the exhumation rate (Supplementary Fig. 3). An error of 10% in the measured age roughly results in a 10% variation of the calculated exhumation rate.

Results

Lineament characteristics

A total of 198 prominent lineaments, most of which trend WNW, N, and NE and enclose rectangular to rhomb-shaped,

upper-crustal domains, were identified between 40° S and 47° S (Figs. 3 and 4). The N-trending lineaments, notably the two known master lineaments and their NE-trending connecting step-over lineaments of the LOFZ, collectively evident by major glacial valleys and fjords, are the longest and morphologically most prominent ones (Figs. 3 and 5). Interestingly, all other lineaments terminate abruptly at the N-trending ones. WNW-trending lineaments are most abundant and transect the entire width of the orogen (Figs. 3 and 4).

In many places, WNW-trending lineaments are curved and truncated as well as displaced by N- and NE-trending lineaments (Figs. 3 and 5). These characteristics point to, respectively, distinct kinematics of upper-crustal deformation, even though some of the truncations may result from the difficulty in tracing lineaments. Truncated lineaments are particularly common in the southern part of the study area (Fig. 5). Strike-separations of displaced WNW-trending lineaments show both, right- and left-lateral apparent displacement components (Fig. 5), with sinistral displacements being less prominent than dextral ones.

Exhumation patterns

Compiled exhumation rates vary mostly between 0.1 and 2.0 mm/yr (Fig. 6). Although the variation in these rates across the LOFZ is regarded as minor by Thomson et al. (2010), their spatial distribution points to differential exhumation in the Southern Andes. Exhumation rates of up to 4.91 mm/yr are concentrated in the central portions of the orogen (Fig. 6). To the East and West, exhumation rates decrease to as low as 0.01 mm/yr. To explore to what extent exhumation is influenced by large-scale (crustal) deformation, the locations of lineament traces are indicated in two E–W and two N–S swath profiles (Fig. 7). The profiles show that gradients in exhumation rates seem to spatially coincide with the location of mapped lineaments, whereby areas that

Fig. 4 Rose diagrams displaying the azimuths of extracted lineaments in 10°-bins with respect to **a** the frequency of orientations and **b** the summed lengths of lineaments. Red, blue and grey dashed lines indicate NE-, NW- and NNE-trending clusters of lineament orientations

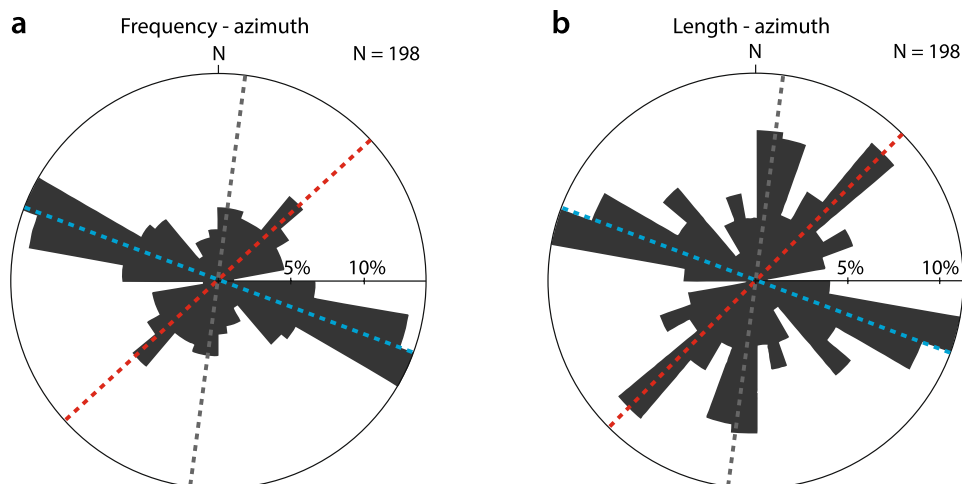
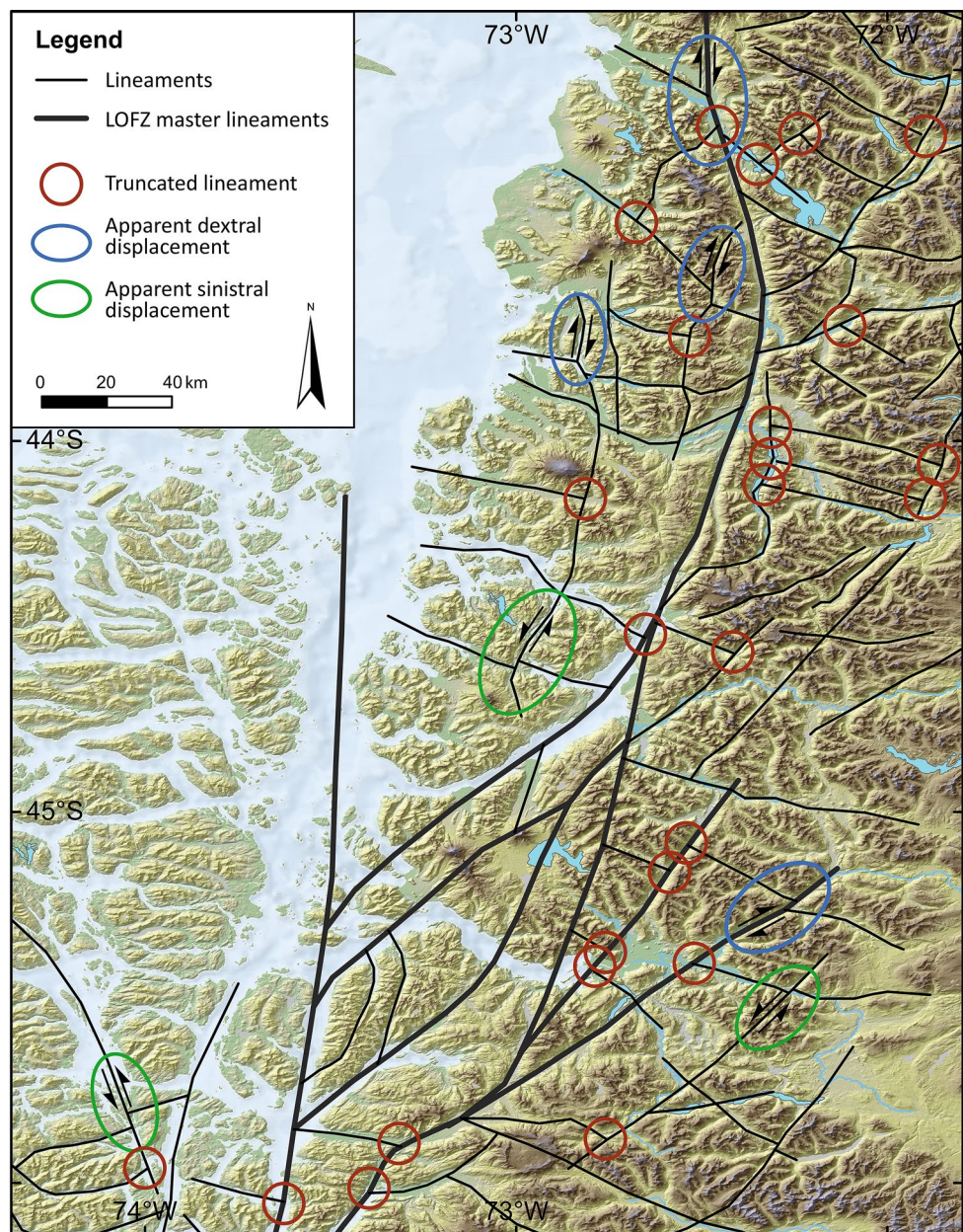


Fig. 5 Lineaments, lineament abutments (red circles) and Horizontal slip components (half arrows) inferred from apparent displacements of lineaments, abutments of lineaments at mutual intersections (red circles) superimposed on topography from the southern portion of the Southern Andean Volcanic Zone. For location of area see Fig. 3



are bordered by lineaments are characterized by uniform exhumation rates (Figs. 6 and 7). Notably, gradients in exhumation are more pronounced at N-trending (orgen-parallel) lineaments than across WNW-trending lineaments.

Discussion

Due to the remoteness and inaccessibility of large parts of the Southern Andes, which render comprehensive, regional structural analyses most challenging (Cembrano et al. 1996, 2000, 2002; Lara et al. 2008), we attempt to constrain the mode of kinematic partitioning in this area through remotely sensed lineaments and published exhumation rates. We will

discuss the pattern of mapped lineaments, the kinematics of fault zones, portrayed by the lineaments, and the relationship between compiled exhumation rates and inferred faults. Based on this data and published fault-kinematic and paleomagnetic studies, we propose a viable alternative to the traditional hypothesis of kinematic partitioning for the Southern Andes.

Lineament pattern

A straightforward result of the lineament extraction from high-resolution DEMs is the fact that prominent lineaments are diverse in trend and distributed over the entire width of the Southern Andes (Fig. 3). Although the individual

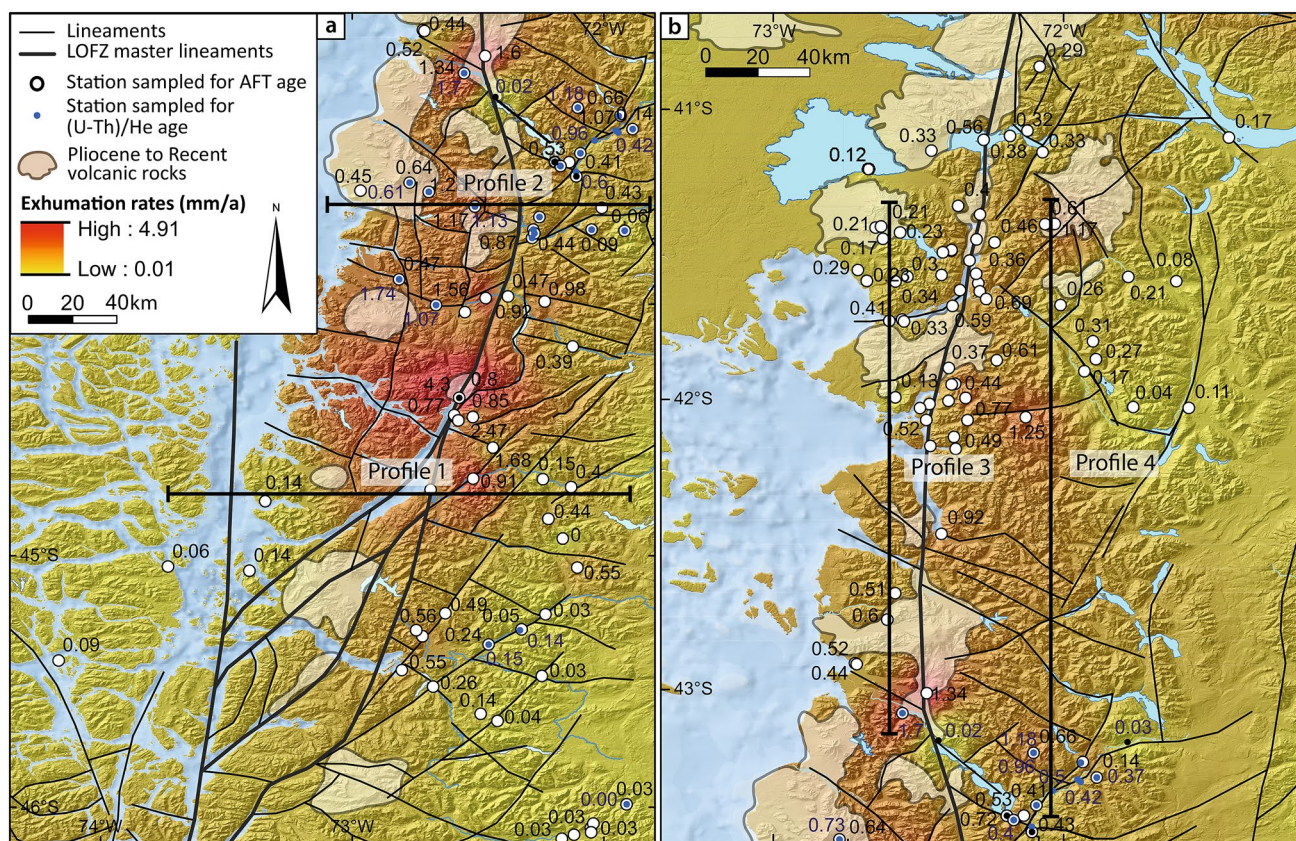


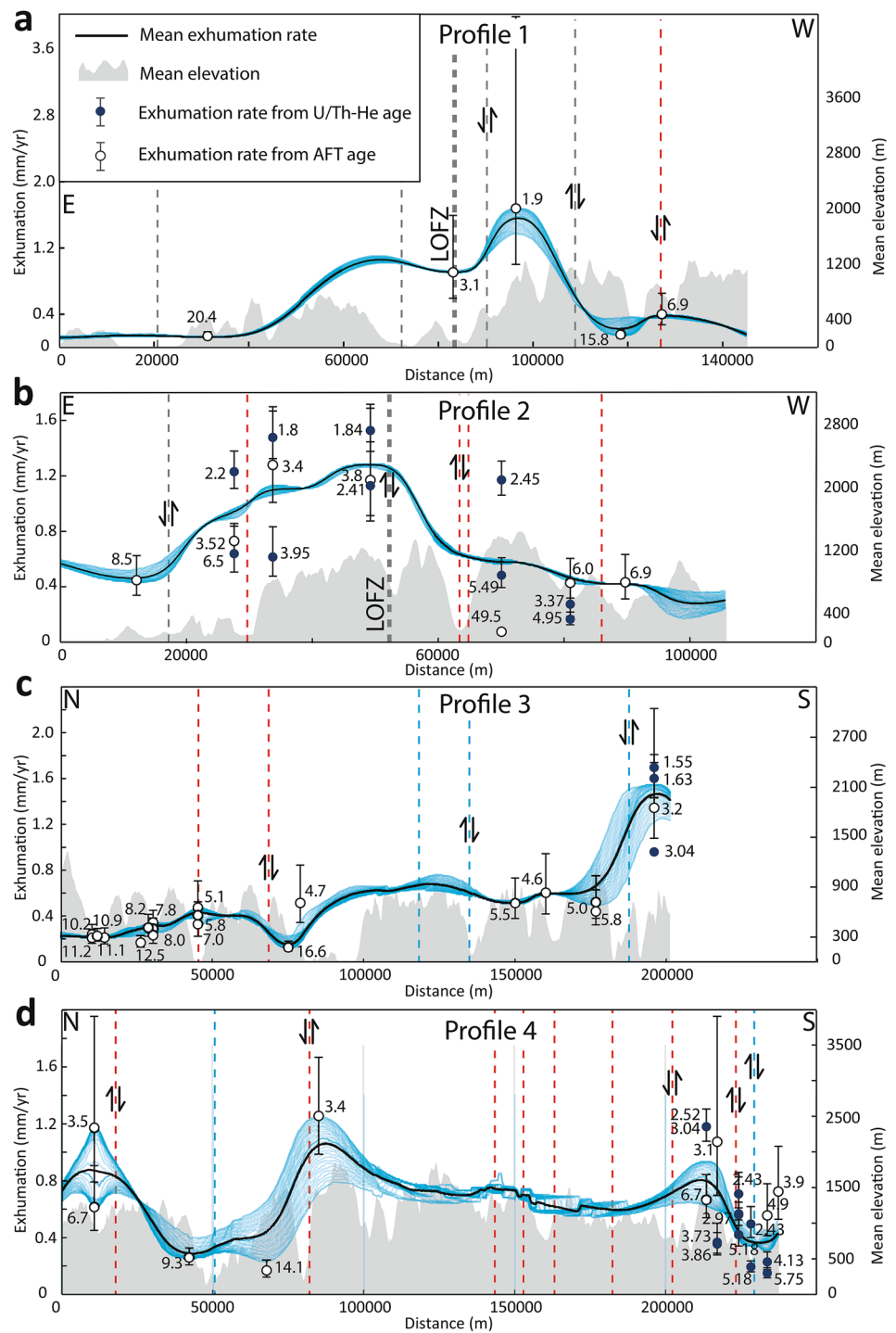
Fig. 6 Interpolated exhumation rates superimposed on DEM from **a** the southern SVZ and **b** the central SVZ. White patches correspond to the extent of Pliocene to recent volcanism simplified from Sernageomin (2003) and Segemar (2017). Black lines indicate the locations of swath profiles in Fig. 7

segments of the LOFZ are part of this lineament pattern, the LOFZ may not have been always as structurally important as conveyed in previous studies. Rather, the network of NE- and WNW-trending lineaments is a ubiquitous structural characteristic of the Southern Andes (Figs. 3 and 4). A fundamental issue regarding the interpretation of these lineaments in terms of deformation is the extent to which they correspond indeed to structural discontinuities, i.e. faults. We, therefore, compared the positions of extracted lineaments to known fault traces at the same locations (Fig. 3). Obviously, the master and associated step-over lineaments of the southern LOFZ have been recognized as faults for a long time (Hervé 1976; Cembrano and Hervé 1993; Cembrano et al. 2000, 2002). Similarly, most prominent WNW-trending lineaments, such as the Gastre and the Mocha Villarica Fault Zone (Fig. 1; Rapela and Pankhurst 1992; Melnick and Echtler 2006), known as Andean transverse

faults (Pérez-Flores et al. 2016; Sielfeld 2019b), have been diagnosed as pre-Andean structural discontinuities that were reactivated during Andean deformation (Yañez and Cembrano 2004; Glodny et al. 2008; Melnick et al. 2009). More importantly, about half of the mapped lineaments do, in fact, correspond to faults (Fig. 3; Diraison et al. 1998; Sernageomin 2003; Lagabriele et al. 2004; Rosenau et al. 2006; Orts et al. 2012; Echaurren et al. 2016). As these lineaments share the same remote sensing characteristics as the rest of the lineaments, which lack direct fault evidence, we are confident that the latter do portray actual faults as well.

Based on the inversion of fault-slip data, Rosenau et al. (2006) proposed a kinematic hypothesis for the presence of margin-parallel dextral and WNW-striking sinistral faults for the northern portion of the SAVZ (see also Hernandez-Moreno et al. 2014). Numerical models corroborate this hypothesis and highlight the kinematic significance

Fig. 7 Swath profiles (width: 10 km) showing interpolated exhumation rates and mean elevation. **a** Profile 1, **b** Profile 2, **c** Profile 3, **d** Profile 4. For location of profiles see Fig. 6. Numbers indicate the ages in Ma. Error bars include errors in the underlying age and ± 3 °C/km deviation from the mean geothermal gradient. Red, blue and grey dashed lines indicate NE-, NW- and N–S-trending lineaments, respectively



of WNW-striking structural discontinuities in this regard (Stanton-Yonge et al. 2016). Although less prominent in the northern SVZ, NE-trending lineaments, many of which are confirmed faults and connected to the LOFZ master faults, are present in the SVZ (Fig. 3). Their kinematic disposition with regard to the LOFZ master faults, reminiscent of synthetic Riedel shears, and shortening directions gleaned from fault-slip analysis (Potent and Reuther 2001; Potent 2003;

Rosenau 2004; Rosenau et al. 2006) point to significant dextral slip components on these faults. These faults and the pattern of mapped lineaments, adhering to faults, fit the kinematic partitioning hypothesis proposed by Rosenau et al. (2006). In summary, oblique plate convergence is not only taken up by dextral strike-slip on the LOFZ. Rather, upper-plate kinematic partitioning of deformation in the Southern Andes has affected the entire orogen and is, to a large extent,

accomplished on WNW-striking structural discontinuities with sinistral slip components and NE-striking discontinuities characterized by dextral slip components.

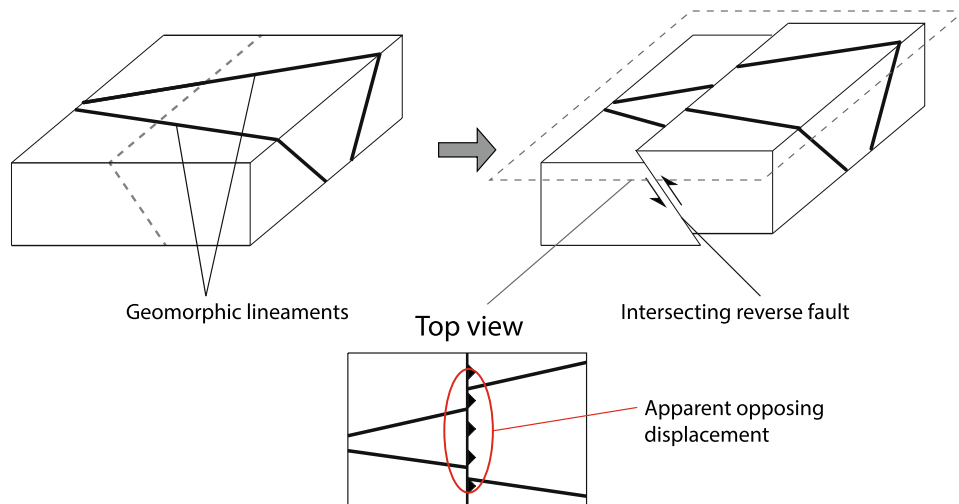
Lineament abutments

Displaced and truncated lineaments in the SVZ (Figs. 3 and 5) offer important insight into the kinematics and the evolution of prominent structural discontinuities. Focussing specifically on lineament abutments between 42° S and 44° S, we note that E- to WNW-trending lineaments are systematically truncated or displaced by northerly and northeasterly trending ones (Fig. 3). Based on the inspection of strike separations of the displaced lineaments, the majority of the slip components on N- and NE-trending lineaments amounts to dextral displacements, in agreement with fault-slip data and models of kinematic partitioning (Cembrano et al. 1996; Rosenau et al. 2006). Dextral displacement of major NW-trending lineaments across the main trace of the LOFZ is observed on multiple occasions (Figs. 3 and 5), in agreement with kinematic data. However, in some places apparent opposite horizontal slip components on the same lineament are recognized, corroborating observations by Cembrano et al. (2000) specifically for the LOFZ. Such cases occur notably where two or more sub-parallel lineaments are apparently displaced in opposite directions on N- and NE-trending lineaments. This lineament configuration can be explained by vertical displacement of oppositely dipping faults abutting on thrust- or reverse faults (Fig. 8) and indicates that the mapped lineaments are indeed the morphologic expressions of surface fault traces. Vertical displacements on faults associated with the LOFZ have been noted by Cembrano et al. (2002); Thomson (2002) and Lara et al. (2008). In fact, abutments of NW-trending lineaments in the southeast portion of the study area (Fig. 4) occur on NE-trending lineaments, which Thomson (2002) interpreted as reverse faults. Judging by the number of identified lineament

abutments (Figs. 3 and 5), vertical displacement on major NW-, NE- and N-striking faults may have been underestimated previously in tectonic models of kinematic partitioning in the Southern Andes. Recognizing field studies such as the ones by Cembrano et al. (2002), Lara et al. (2008), and Arancibia et al. (1999), we conclude that the LOFZ is not characterized by dextral strike-slip only, and that any hypothesis on kinematic partitioning in the Southern Andes needs to honour significant vertical displacement components on margin-parallel structural discontinuities.

A second important aspect of documented lineament abutments concerns the evolution of the lineament (fault) sets. Based on our observations, WNW-trending lineaments are truncated by N-trending lineaments, including step-over lineaments, of the LOFZ which may point to the former arc-oblique lineaments predating the LOFZ. This may indicate that orogen-scale, upper-crustal faulting in the Southern Andes has adhered to the classical model of brittle fault development in a fault zone, i.e., initial distributed faulting decreases progressively and culminates in the localisation of a few master faults (Stanchits et al. 2011). By analogy, distributed faulting affecting the entire width of the Andean orogen may be followed by localization of deformation on a few master faults in the orogen center. In fact, WNW- and NE-striking faults were active in Neogene times (Rosenau et al. 2006) and, thus, started to be active before the LOFZ master faults at about 4 Ma (Cembrano et al. 2002) and many of the modern volcanic centers in the SVZ. We speculate that arc magmatism through thermal softening of crust rendered localization of deformation to the center of the SVZ and culminated in the formation of the LOFZ (Fig. 1). Progressive localization of deformation on the LOFZ (Astudillo-Sotomayor et al. 2021) may have been also prompted by a change in the tectonic style of deformation during the Neogene. Structural studies of the eastern sector of the Southern Andes indicate a Cretaceous and a late Miocene phase of enhanced shortening, which lead to

Fig. 8 Schematic diagram illustrating sense of vertical slip components inferred from horizontal strike separations of (oppositely) dipping planar structures displaced on a reverse fault



the formation of thrust and reverse faults in the retroarc (Orts et al. 2012, 2015; Echaurren et al. 2016). The subsequent cessation of shortening in the retroarc, may well have aided in the observed present-day localization of deformation on the master faults of the LOFZ. Alternatively, enhanced glaciation during the Pliocene may have promoted an orogen-wide retreat of deformation to its core which facilitates the LOFZ (Thomson et al. 2010). However, recent crustal earthquakes obtained through temporary seismic networks in the arc-region of the Southern Andes demonstrate the present activity of major margin-oblique faults aside from the main LOFZ (Lange et al. 2008) indicating that distributed deformation to some degree has continued to this day (Sielfeld et al. 2019a).

Exhumation pattern

Interpolated rock exhumation rates highlight respective variations in the Southern Andes (Fig. 6). High exhumation rates of up to 4.91 mm/yr are evident in the central, topographically most elevated portions of the orogen. These rates are, on the one hand, attributed to denudation by enhanced glacial activity during the Pliocene and Pleistocene (Thomson et al. 2010; Christeleit et al. 2017). On the other hand, exhumation is maximal to the west of the highest elevations, likely due to orographic precipitation (Fig. 7a, b). Anomalous young AFT ages are reported from the vicinity of the LOFZ and were attributed to the influence of an enhanced upper-crustal heat flow caused by magmatism and associated advection of hot fluids along fracture zones (Thomson 2002). Thus, high exhumation rates calculated from young AFT and (U–Th)/He ages close to the LOFZ and the present-day volcanic arc (Fig. 6) may have resulted from a higher geothermal gradient than used for our calculation. As samples of various ages experience the same change in exhumation rate with changing geothermal gradient (Supplementary Fig. 1), a change in the geothermal gradient results in an overall increase or decrease of all exhumation rates. Similarly, an enhanced erosion at 44° S due to an increase in precipitation, as proposed by Herman and Brandon (2015), would be expected to produce a widespread increase in recorded rock exhumation at the respective area. Consequently, considerable latitudinal and longitudinal variations in exhumation rates over few tens of kilometers (Fig. 7) may indicate that exhumation rates are overestimated, but processes such as local differential surface uplift and erosion also govern intrarc variations in rock exhumation.

The spatial correspondence of mapped lineaments with gradients in the interpolated surface of modelled exhumation rates indicates a considerable influence of large-scale (crustal) deformation on rock exhumation (Fig. 7) in addition to an influence of late Miocene and Pliocene enhanced glaciation on exhumation rates (Thomson et al. 2010;

Christeleit et al. 2017). More specifically, differential rock uplift, i.e. vertical extrusion of rock, appears to be associated with reverse and thrust faults marked by the respective lineaments, notably N-trending ones (Fig. 7a, b). Moreover, orogen-parallel exhumation trends display plateaus of high exhumation rates and narrow depressions of low exhumation rates, both bordered by lineaments (Fig. 7c, d). These observations agree with differential rock uplift of lineament-bound, upper-crustal domains. The pattern of compiled exhumation rates in combination with new lineament (fault) data provide evidence for widespread reverse faulting notably on N-trending faults, possibly enhanced through isostatic uplift due to glacial retreat in the Southern Andes. As the variations in exhumation rates across the Southern Andes are almost exclusively constrained by Miocene to Pliocene AFT and (U–Th)/He ages, reverse faulting occurred likely during the late Miocene and Pliocene. These observations agree with widespread Miocene reverse faulting along the LOFZ (Arancibia et al. 1999; Thomson 2002; Cembrano et al. 2000; 2002) and the eastern slope of the Southern Andes (Diraison et al. 1998; Orts et al. 2015; Echaurren et al. 2016). Horizontal shortening as reported for the North Patagonian fold-and-thrust belt (Orts et al. 2012; Echaurren et al. 2016) may have affected the entire Southern Andes and, based on AFT and (U–Th)/He ages, may have continued into the Pliocene.

Revised mode of kinematic partitioning in the Southern Andes

Recent kinematic, geochronologic and paleomagnetic studies question the traditional concept of kinematic partitioning in the Southern Andes, in which the LOFZ is viewed as the dominant fault zone accomplishing predominately horizontal shearing (Thomson 2002; Rosenau et al. 2006; Hernandez-Moreno et al. 2014; Georgieva et al. 2016). In contrast to the traditional concept of deformation partitioning, our structural analysis is consistent with previous structural studies (Diraison et al. 1998; Rosenau et al. 2006; Hernandez-Moreno et al. 2014). Notably, our analysis calls for Miocene distributed deformation on margin-parallel, NE-striking and WNW-striking faults, which continued to be active in Pliocene times. Collectively, horizontal and vertical shear components on these faults affected the entire southern Andean orogen (Fig. 9). Rock uplift and differential vertical displacements on the LOFZ and other margin-parallel faults are maximal in the central portions of the orogen. The results indicate that the Southern Andes took up oblique plate convergence by horizontal shortening, crustal thickening and mostly dextral strike-slip during the Miocene and Pliocene, which fit the tectonic model of dextral transpression (Harland 1971; Sanderson and Marchini 1984; Robin and Cruden 1994; Dewey et al. 1998) on the

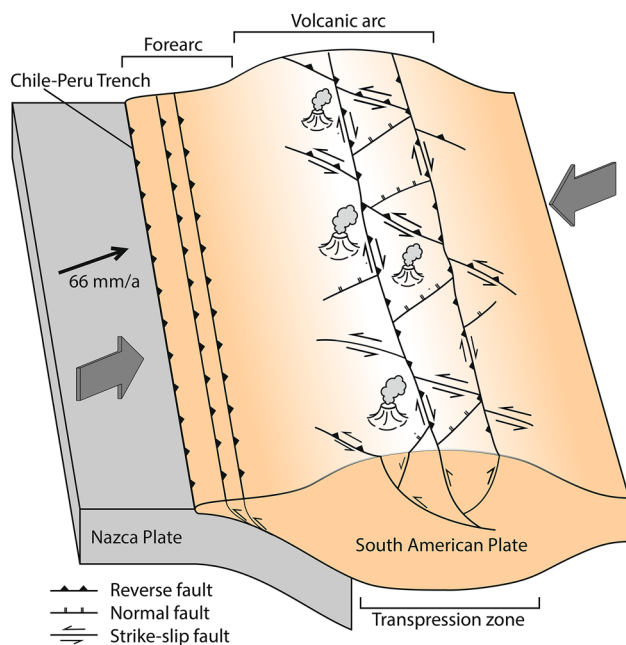


Fig. 9 Schematic block diagram depicting kinematic partitioning amounting to dextral transpression in the Southern Andes

orogen scale (Fig. 9). As mentioned above, the observed present-day concentration of strike-slip on the LOFZ may have resulted from decreased shortening rates since the Pliocene. In this context, transpression may well have been superseded mostly by dextral displacement on arc-parallel master faults of the LOFZ (Lange et al. 2008). As oblique slip and reverse displacement still occur today (e. g. Lara et al. 2008; Sielfeld et al. 2019a), we regard the southern Andean orogen as a crustal-scale transpression zone with ill-defined zone boundaries.

Conclusions

Identification of distinct lineament sets, portraying traces of upper-crustal faults or fault zones, and reassessment of low-T thermochronology data requires reconsideration of kinematic partitioning in the Southern Andes. We find that oblique plate convergence in the Miocene to Pliocene has been accommodated by (1) distributed deformation affecting the entire orogen, (2) three lineament (fault) sets accomplishing chiefly margin-parallel dextral displacement and horizontal shortening and (3) rock uplift that is maximal in the orogen center. These characteristics amount to dextral transpression on the orogen scale and indicate that previously the component of horizontal shortening was underestimated, whereas the kinematic role of the Liquiñe-Ofqui Fault Zone as the sole strike-slip fault was overestimated. Pliocene transpressive deformation in the Southern Andes,

inferred from AFT and (U–Th)/He ages indicates that the currently observed strike-slip deformation within the Southern Andes may only have begun during the late Pliocene.

Supplementary Information The online version contains supplementary material available at <https://doi.org/10.1007/s00531-021-02068-y>.

Acknowledgements This work was supported by the German Science Foundation (grant Ri-916/17-1). Reviews by A. Stevens Goddard and an anonymous person are greatly appreciated and helped to clarify the content of this contribution. Digital elevation models were obtained from Japan's Ministry of Economy, Trade, and Industry (METI) and NASA.

Funding Open Access funding enabled and organized by Projekt DEAL. This work was supported by the German Science Foundation (grant Ri-916/17-1).

Availability of data and material Not applicable.

Code availability Not applicable.

Declarations

Conflict of interest The authors declare that they have no conflict of interest.

Open Access This article is licensed under a Creative Commons Attribution 4.0 International License, which permits use, sharing, adaptation, distribution and reproduction in any medium or format, as long as you give appropriate credit to the original author(s) and the source, provide a link to the Creative Commons licence, and indicate if changes were made. The images or other third party material in this article are included in the article's Creative Commons licence, unless indicated otherwise in a credit line to the material. If material is not included in the article's Creative Commons licence and your intended use is not permitted by statutory regulation or exceeds the permitted use, you will need to obtain permission directly from the copyright holder. To view a copy of this licence, visit <http://creativecommons.org/licenses/by/4.0/>.

References

- Angermann D, Klotz J, Reigber C (1999) Space-geodetic estimation of the Nazca-South America Euler vector. *Earth Planet Sci Lett* 171:329–334
- Arancibia G, Cembrano J, Lavenu A (1999) Transpresión dextral y partición de la deformación en la Zona de Falla Liquiñe-Ofqui, Aisén, Chile (44–45°S). *Rev Geol Chile* 26:3–22
- Astudillo-Sotomayor L, Jara-Muñoz J, Melnick D, Cortés-Aranda J, Tassara A, Strecker MR (2021) Fast Holocene slip and localized strain along the Liquiñe-Ofqui strike-slip fault system. *Chile Sci Rep* 11:5970
- Beck ME (1983) On the mechanism of tectonic transport in zones of oblique subduction. *Tectonophysics* 93:1–11
- Beck ME (1991) Coastwise transport reconsidered: lateral displacements in oblique subduction zones, and tectonic consequences. *Phys Earth Planet Inter* 68:1–8
- Beck ME, Burmester RF, Steele BC (1998) Paleomagnetism of probably remagnetized late Mesozoic volcanic rocks near Lago Verde, Aisén, Southern Chile. *Andean Geol* 25:153–163

- Beck ME, Burmester RF, Cembrano J, Drake R (2000) Paleomagnetism of the North Patagonian Batholith, southern Chile. An exercise in shape analysis. *Tectonophysics* 326:185–202
- Catalán N, Bataille K, Araya R (2017) Depth-dependent geometry of the Liquiñe-Ofqui fault zone and its relation to paths of slab-derived fluids. *Geophys Res Lett* 44:916–920
- Cembrano J, Hervé F (1993) The Liquiñe Ofqui Fault Zone: A major Cenozoic strike slip duplex in the southern Andes. In: *Off. de la Rech. Sci. et Tech. d'Outre-mer (ORSTOM)* (ed) *Andean geodynamics: extended abstracts*, OSTROM, Paris, pp 175–178
- Cembrano J, Beck ME, Burmester RF, Rojas C, Garcia A, Herve F (1992) Paleomagnetism of lower Cretaceous rocks from east of the Liquiñe-Ofqui fault zone, southern Chile: evidence of small in-situ clockwise rotations. *Earth Planet Sci Lett* 113:539–551
- Cembrano J, Hervé F, Lavenu A (1996) The Liquiñe-Ofqui fault zone: a long lived intraarc fault system in southern Chile. *Tectonophysics* 259:55–66
- Cembrano J, Schermer E, Lavenu A, Sanhueza A (2000) Contrasting nature of deformation along an intra-arc shear zone, Liquiñe-Ofqui fault zone, southern Chilean Andes. *Tectonophysics* 319:129–149
- Cembrano J, Lavenu A, Reynolds P, Arancibia G, López G, Sanhueza A (2002) Late Cenozoic transpressional ductile deformation north of the Nazca—South America—Antarctica triple junction. *Tectonophysics* 354:289–314
- Chemenda A, Lallemand S, Bokun A (2000) Strain partitioning and interplate friction in oblique subduction zones: constraints provided by experimental modeling. *J Geophys Res* 105:5567–5581
- Chen W-Y, Wu J, Suppe J (2019) Southwards propagation of Nazca subduction along the Andes. *Nature* 565:441–447
- Christeleit EC, Brandon MT, Shuster D (2017) Miocene development of alpine glacial relief in the Patagonian Andes, as revealed by low-temperature thermochronometry. *Earth Planet Sci Lett* 460:152–163
- Davies BJ, Darvill CM, Lovell H et al (2020) The evolution of the Patagonian Ice Sheet from 35 ka to the present day (PATICE). *Earth-Sci Rev* 204:103152
- Dewey JF, Lamb SH (1992) Active tectonics of the Andes. *Tectonophysics* 205:79–95
- Dewey JF, Holdsworth RE, Strachan RA (1998) Transpression and transtension zones. *Geol Soc London Spec Publ* 135:1–14
- Diraison M, Cobbold PR, Rossello EA, Amos AJ (1998) Neogene dextral transpression due to oblique convergence across the Andes of northwestern Patagonia, Argentina. *J South Am Earth Sci* 11:519–532
- Diraison M, Cobbold PR, Gapais D, Rosello EA, Le Corre C (2000) Cenozoic crustal thickening, wrenching and rifting in the foothills of the southernmost Andes. *Tectonophysics* 216:91–119
- Echaurren A, Folguera A, Gianni G, Orts D, Tassara A, Encinas A, Giménez M, Valencia V (2016) Tectonic evolution of the North Patagonian Andes (41°–44° S) through recognition of syntectonic strata. *Tectonophysics* 677–678:99–114
- Fick SE, Hijmans RJ (2017) WorldClim 2: new 1-km spatial resolution climate surfaces for global land areas. *Int J Climatol* 37:4302–4315
- Fitch TJ (1972) Plate convergence, transcurrent faults, and internal deformation adjacent to southeast Asia and the western Pacific. *J Geophys Res* 77:4432–4460
- García A, Beck ME, Burmester R, Munizaga F, Herve F (2011) Paleomagnetic reconnaissance of the region de los Lagos, southern Chile, and its tectonic implications. *Revista Geológica Chile* 15:13–30
- Georgieva V, Melnick D, Schildgen TF, Ehlers TA, Lagabriele Y, Enkelmann E, Strecker MR (2016) Tectonic control on rock uplift, exhumation, and topography above an oceanic ridge collision: Southern Patagonian Andes (47°S), Chile. *Tectonics* 35:1317–1341
- Giacosa RE, Heredia C (2004) Structure of the North Patagonian thick-skinned fold-and-thrust belt, southern central Andes, Argentina (41°–42°S). *J South Am Earth Sci* 18:61–72
- Glodny J, Echter H, Collao S, Ardiles M, Burón P, Figueroa O (2008) Differential Late Paleozoic active margin evolution in South-Central Chile (37°S–40°S)—the Lanalhue Fault Zone. *J S Am Earth Sci* 26:397–411
- Hamza VM, Muñoz M (1996) Heat flow map of South America. *Geothermics* 25:599–621
- Harland WB (1971) Tectonic transpression in Caledonian Spitzbergen. *Geol Mag* 108:27–42
- Hein AS, Dunai TJ, Hulton NRJ, Xu S (2011) Exposure dating outwash gravels to determine the age of the greatest Patagonian glaciations. *Geology* 39:103–106
- Herman F, Brandon M (2015) Mid-latitude glacial erosion hotspot related to equatorial shifts in southern Westerlies. *Geology* 43:987–990
- Hernandez-Moreno C, Speranza F, Di Ciara A (2014) Understanding kinematics of intra-arc transcurrent deformation: Paleomagnetic evidence from the Liquiñe-Ofqui fault zone (Chile, 38–41°S). *Tectonics* 33:1964–1988
- Hervé M (1976) Estudio geológico de la falla Liquiñe-Reloncaví en la área de Liquiñe: Antecedentes de un movimiento transcurrente (Provincia de Valdivia). *Actas Congreso Geológico Chileno* 1:39–56
- Hervé F, Pankhurst RJ, Drake R, Beck ME, Mpodozis C (1993) Granite generation and rapid unroofing related to strike-slip faulting, Aysén, Chile. *Earth Planet Sci Lett* 120:375–386
- Hoffmann-Rothe A, Kukowski N, Dresen N, Echter G, Oncken O, Klotz J, Scheuber E, Kellner A (2006) Oblique convergence along the Chilean margin: partitioning, margin-parallel faulting and force interaction at the plate interface. In: Oncken O (ed) *The Andes: Active Subduction Orogeny*. Springer, Berlin, Heidelberg, pp 125–146
- Jarrard RD (1986) Relations among subduction parameters. *Rev Geophys* 24:217–284
- Kimura G (1986) Oblique subduction and collision: Forearc tectonics of the Kuril arc. *Geology* 14:404–407
- Klotz J, Khazaradze G, Angermann D, Reigber C, Perdomo R, Cifuentes O (2001) Earthquake cycle dominates contemporary crustal deformation in Central and Southern Andes. *Earth Planet Sci Lett* 193:437–446
- Lagabriele Y, Suarez M, Rossello EA, Herail G, Martinod J, Regnier M, de la Cruz R (2004) Neogene to Quaternary tectonic evolution of the Patagonian Andes at the latitude of the Chile Triple Junction. *Tectonophysics* 385:211–241
- Lange D, Cembrano J, Rietbrock A, Haberland C, Dahm T, Bataille K (2008) First seismic record for intra-arc strike-slip tectonics along the Liquiñe-Ofqui fault zone at the obliquely convergent plate margin of the southern Andes. *Tectonophysics* 455:14–24
- Lara LE, Cembrano J, Lavenu A (2008) Quaternary vertical displacement along the Liquiñe-Ofqui fault zone: differential uplift and coeval volcanism in the Southern Andes? *Int Geol Rev* 50:975–993
- Lavenu A, Cembrano J (1999) Compressional- and transpressional-stress pattern for Pliocene and Quaternary brittle deformation in fore arc and intra-arc zones (Andes of central and southern Chile). *J Struct Geol* 21:1669–1691
- McCaffrey R (1992) Oblique plate convergence, slip vectors, and forearc deformation. *J Geophys Res* 97:8905–8915
- Melnick D, Echter HP (2006) Morphotectonic and geologic digital map compilations of the south-central Andes (36°–42°S). In: Oncken O (ed) *The Andes: Active Subduction Orogeny*. Springer, Berlin, Heidelberg, pp 125–146

- Melnick D, Bookhagen B, Strecker MR, Echtler HP (2009) Segmentation of megathrust rupture zones from fore-arc deformation patterns over hundreds to millions of years, Arauco peninsula. *Chile J Geophys Res* 114:B01407
- Moreno M, Melnick D, Rosenau M, Bolte J, Klotz J, Echtler H, Baez J, Bataille K, Chen J, Bevis M, Hase H, Oncken O (2011) Heterogeneous plate locking in the South-Central Chile subduction zone: Building up the next great earthquake. *Earth Planet Sci Lett* 305:413–424
- Orts D, Folguera A, Encinas A, Ramos M, Tobal J, Ramos VA (2012) Tectonic development of the North Patagonian Andes and their related Miocene foreland basin (41°30'–43°S). *Tectonics* 31:TC3012
- Orts D, Folguera A, Giménez M, Ruiz F, Rojas Vera EA, Lince Klinger F (2015) Cenozoic building and deformational processes in the North Patagonian Andes. *J Geodyn* 86:26–41
- Pardo-Casas F, Molnar P (1987) Relative motion of the Nazca (Farallon) and South American plates since Late Cretaceous times. *Tectonics* 6:233–248
- Pérez-Flores P, Cembrano J, Sánchez-Alfaro P, Veloso E, Arancibia G, Roquer T (2016) Tectonics, magmatism and paleo-fluid distribution in a strike-slip setting: insights from the northern termination of the Liquiñe-Ofqui fault System, Chile. *Tectonophysics* 680:192–210
- Pérez-Peña JV, Al-Awabdeh M, Azañón JM, Galve JP, Booth-Rea G, Notti D (2017) SwathProfiler and NProfiler: two new ArcGIS Add-ins for the automatic extraction of swath and normalized river profiles. *Comput Geosci* 104:135–150
- Potent S (2003) Kinematik und Dynamik neogener Deformationssprozesse des südzentralchilenischen Subduktionssystems, nördlichste Patagonische Anden (37°–40°S), Unpublished Dissertation, Universität Hamburg, Germany
- Potent S, Reuther C-D (2001) Neogene Deformationsprozesse im aktiven magmatischen Bogen Südzentralchiles zwischen 37°S und 39°S. *Mitteilungen Des Geologisch-Paläontologischen Instituts* 85:1–22
- Rapela CW, Pankhurst RJ (1992) The granites of northern Patagonia and the Gastre Fault System in relation to the break-up of Gondwana. *Geol Soc Spec Pub* 68:209–220
- Reutter K-J, Scheuber E, Chong G (1996) The precordilleran fault system of Chuquicamata, Northern Chile: evidence for reversals along arc-parallel strike-slip faults. *Tectonophysics* 259:213–228
- Riller U, Oncken O (2003) Growth of the central Andean Plateau by tectonic segmentation is controlled by the gradient in crustal shortening. *J Geol* 111:367–384
- Robin P-YF, Cruden AR (1994) Strain and vorticity patterns in ideally ductile transpression zones. *J Struct Geol* 16:447–466
- Rojas C, Beck ME, Burmester R (1994) Paleomagnetism of the mid-Tertiary Ayacara Formation, southern Chile: counterclockwise rotation in a dextral shear zone. *J South Am Earth Sci* 7:45–56
- Rosenau M (2004) Tectonics of the southern Andean intra-arc zone (38°–42°S), PhD thesis. Freie Universität Berlin
- Rosenau M, Melnick D, Echtler H (2006) Kinematic constraints on intra-arc shear and strain partitioning in the southern Andes between 38°S and 42°S latitude. *Tectonics* 25:TC4013
- Sanderson DJ, Marchini WRD (1984) Transpression. *J Struct Geol* 6:449–458
- Scheuber E, González G (1999) Tectonics of the Jurassic-early Cretaceous magmatic arc of the north Chilean Coastal Cordillera (22°–26°S): a story of coupling and decoupling in the subduction zone. *Tectonics* 18:895–910
- Segemar (2017) Unidad Geológica 2.5M: Edición 1.0. Servicio Geológico Minero Argentino, San Martín, Argentina. <https://sigam.segemar.gov.ar/visor/index.html?mapa=11>
- Sernageomin S (2003) Mapa Geológico de Chile: Versión digital, No 4, CD-ROM versión 1.0. Servicio Nacional de Geología y Minería. Publicación Geológica Digital, Santiago de Chile, Chile
- Sielfeld G, Lange D, Cembrano J (2019a) Intra-arc crustal seismicity: seismotectonic implications of the Southern Andes Volcanic Zone, Chile. *Tectonics* 38:552–578
- Sielfeld G, Ruz J, Brogi A, Cembrano J, Stanton-Yonge A, Pérez-Flores P, Iturrieta P (2019b) Oblique-slip tectonics in an active volcanic chain: a case study from the Southern Andes. *Tectonophysics* 770:228221
- Somoza R (1998) Updated Nazca (Farallon)–South America relative motions during the last 40 My: implications for mountain building in the central Andean region. *J South Am Earth Sci* 11:211–215
- Stanchits S, Mayr S, Shapiro S, Dresen G (2011) Fracturing of porous rock induced by fluid injection. *Tectonophysics* 503:129–145
- Stanton-Yonge A, Griffith WA, Cembrano J, St. Julien R, Iturrieta P (2016) Tectonic role of margin-parallel and margin-transverse faults during oblique subduction in the Southern Volcanic Zone of the Andes: insights from Boundary Element Modeling. *Tectonics* 35:1990–2013
- Thomson SN (2002) Late Cenozoic geomorphic and tectonic evolution of the Patagonian Andes between latitudes 42 and 46 S: an appraisal based on fission-track results from the transpressional intra-arc Liquiñe-Ofqui fault zone. *Geol Soc Am Bull* 114:1159–1173
- Thomson SN, Brandon MT, Tomkin JH, Reiners P, Vásquez C, Wilson N (2010) Glaciation as a destructive and constructive control on mountain building. *Nature* 467:313–317
- Tikoff B, Teyssier C (1994) Strain modeling of displacement field partitioning in transpressional orogens. *J Struct Geol* 16:1575–1588
- Wang K, Hu Y, Bevis M, Kendrick E, Smalley R, Vargas RB, Lauría E (2007) Crustal motion in the zone of the 1960 Chile earthquake: Detangling earthquake-cycle deformation and forearc-sliver translation. *Geochem Geophys Geosyst* 8:Q10010
- Watson DF, Philip GM (1985) A refinement of inverse distance weighted interpolation. *Geoprocessing* 2:315–327
- Willet SD, Brandon MT (2013) Some analytical methods for converting thermochronometric age to erosion rate. *Geochem Geophys Geosyst* 14:209–222
- Yañez G, Cembrano J (2004) Role of viscous plate coupling in the late Tertiary Andean tectonics. *J Geophys Res* 109:B02407